

PAPER • OPEN ACCESS

First-principles DFT insights into the structural, elastic, and optoelectronic properties of α and β -ZnP₂: implications for photovoltaic applications

To cite this article: Aleksandar Živkovi *et al* 2019 *J. Phys.: Condens. Matter* **31** 265501

View the [article online](#) for updates and enhancements.



IOP | ebooks™

Bringing together innovative digital publishing with leading authors from the global scientific community.

Start exploring the collection—download the first chapter of every title for free.

First-principles DFT insights into the structural, elastic, and optoelectronic properties of α and β -ZnP₂: implications for photovoltaic applications

Aleksandar Živković^{1,4} , Barbara Farkaš^{1,4}, Veikko Uahengo², Nora H de Leeuw¹ and Nelson Y Dzade^{1,3} 

¹ School of Chemistry, Cardiff University, Main Building, Park Place, Cardiff, CF10 3AT, United Kingdom

² Department of Chemistry and Biochemistry, University of Namibia, 340 Mandume Ndemufayo Avenue, Windhoek 9000, Namibia

E-mail: DzadeNY@cardiff.ac.uk

Received 21 January 2019, revised 27 February 2019

Accepted for publication 19 March 2019


Published 15 April 2019



Abstract

Binary II–V semiconductors are highly optically active materials, possess high intrinsic mechanical and chemical durability, and have electronic properties ideal for optoelectronic applications. Among them, zinc diphosphide (ZnP₂) is a promising earth-abundant absorber material for solar energy conversion. We have investigated the structural, mechanical, and optoelectronic properties of both the tetragonal (α) and monoclinic (β) phases of ZnP₂ using standard, Hubbard-corrected and screened hybrid density functional theory methods. Through the analysis of bond character, band gap nature, and absorption spectra, we show that there exist two polymorphs of the β phase (denoted as β_1 and β_2) with distinct differences in the photovoltaic potential. While β_1 exhibits the characteristics of metallic compounds, β_2 is a semiconductor with predicted thin-film photovoltaic absorbing efficiency of almost 10%. The α phase is anticipated to be an indirect gap material with a calculated efficiency limited to only 1%. We have also analysed and gained insights into the electron localization function, projected density of states and projected crystal orbital Hamilton populations for the analogue bonds between the α and β -ZnP₂. In light of these calculations, a number of previous discrepancies have been solved and a solid ground for future employment of zinc diphosphides in photovoltaics has been established.

Keywords: electronic structure, semiconductors, photovoltaics, density functional theory

 Supplementary material for this article is available [online](#)

(Some figures may appear in colour only in the online journal)

1. Introduction

Photovoltaic (PV) technology which makes use of the super-abundant and freely available Sun's energy to generate electricity has obvious economic, environmental and societal benefits. However, to achieve significant market penetration,

PV devices have to be efficient and composed of cheap and readily available materials. Different alternatives to the dominating crystalline silicon are being investigated, with semi-conducting thin film technologies now providing almost 10% of the total photovoltaic production capacity. Nevertheless, the scarcity, cost, and toxicity associated with the constituent elements counterbalance the high power conversion efficiencies (PCE) commonly associated with these devices [1].

³ Author to whom any correspondence should be addressed.

⁴ These authors contributed equally.



Semiconducting II–V compounds are formed from comparatively inexpensive and non-toxic elements (e.g. Zn, N, P), which makes them attractive for large-scale PV applications. Amongst those, Zn_3P_2 and ZnP_2 are promising solar spectrum absorbers due to their favourable band gap energy values. Furthermore, they are mechanically and chemically stable, highly optically active (birefringence and rotation of the polarisation plane), possess long minority-carrier diffusion lengths, and have strong light absorption in the visible region [2–6]. Zinc diphosphide (ZnP_2), which crystallizes in two distinct modifications: tetragonal $\alpha\text{-ZnP}_2$ (red) and monoclinic $\beta\text{-ZnP}_2$ (black), received little attention despite both phases having narrow band gaps and multivalley conduction and valence bands which result in high thermopower and, combined with the non-cubic symmetry, strong anisotropic optical properties with large birefringence [7]. Moreover, the power production potential of $\beta\text{-ZnP}_2$, based on the world resource estimates of its elemental constituents, is predicted to be 3.5×10^5 and 2.0×10^4 times larger than InP and GaAs, respectively, for cells operating at 10% efficiency [8]. These features make zinc diphosphides prospective candidates for optoelectronic applications and next-generation solar energy conversion materials.

The development of ZnP_2 materials as efficient and cost-effective solar absorbers requires an atomic-level understanding of their fundamental properties (e.g. band gap energies, near-edge band structures, dielectric function, optical absorption coefficients). However, the basic mechanical and structural characteristics, as well as electronic and optical features of zinc diphosphides are poorly understood and inconclusive.

The crystal structure of $\alpha\text{-ZnP}_2$ was first reported by Stackelberg and Paulus in 1935 [9] as a tetragonal cell containing eight formula units, with each Zn atom surrounded by four P atoms and each P atom surrounded by two Zn and two P atoms. This structure was experimentally confirmed in the 1960s and 1980s by a few groups [7, 10, 11], and again in 2003 by Zanin *et al* [12]. Elastic constants have been found to depend linearly on temperature in the range from 78 to 400 K, with occasional interruption areas of 10–20 K width [13]. From earlier experimental studies of optoelectronic properties of ZnP_2 materials, it is believed that the top of the valence band of $\alpha\text{-ZnP}_2$ is located at the Γ point and the energy gap is indirect but dipole forbidden [14]. Pressure dependence experiments for vibrational Raman modes, as well as for the band gap of $\alpha\text{-ZnP}_2$, showed very small changes (~ 0.02 eV) up to 100 kBar [15]. The temperature dependence of the band gap was also reported [15] with a decrease of 0.25 eV in the range from 4.2 to 400 K. Overall, experimental values for the indirect band gap of $\alpha\text{-ZnP}_2$ fall within the range of 2.1–2.3 eV [16, 17]. Theoretical investigations, from pseudopotential methods to more accurate density functional theory calculations, although in fairly good agreement with experiments in the description of structural and elastic properties, failed to accurately reproduce the fundamental electronic band gap (underestimating it by ~ 0.5 eV) [18–20]. Additionally, the nature of the transition has been wrongly modelled as direct.

In contrast, since it was first synthesized, $\beta\text{-ZnP}_2$ caused controversy regarding the order of Zn and P atoms. The new crystal form discovered by Hegyi *et al* [7], monoclinic and black in colour, was suggested to have a fraction of Zn and P atoms bonded to one Zn and three P atoms. However, experimental studies conducted by Fleet [21] suspected the existence of Zn–Zn bonds which they attributed to the insufficiency of high quality intensity data. Further studies have discarded the initial structure and reported each P atom to have two bonds to Zn and two to P atoms, similarly to the α -phase [12, 22]. Changes in the elastic properties that follow the temperature alternations are analogous to those in $\alpha\text{-ZnP}_2$ [13]. From the experimental analysis of the electronic properties, the lowest energy gap of the $\beta\text{-ZnP}_2$ is identified to be direct [23], with conduction band composed mainly from Zn and the valence band mainly from P ion states [4]. Strong temperature dependence was observed for all optical functions of $\beta\text{-ZnP}_2$, partially induced by the crystal's high anisotropy [17]. Experimental band gap values for $\beta\text{-ZnP}_2$ were reported in the range 1.33–1.60 eV [4, 17]. As in the case of $\alpha\text{-ZnP}_2$, theoretical energies of band gap are smaller than measured values by almost 0.8 eV, but with a reasonable reproduction of structural and mechanical properties [20].

Due to the relative dearth of theoretical works and inconsistency in existing ones, it is clear that a comprehensive study of both $\alpha\text{-ZnP}_2$ and $\beta\text{-ZnP}_2$ is needed to reveal their possible PV potential. Therefore, density functional theory calculations with standard GGA, Hubbard-corrected GGA+ U and screened hybrid DFT methods have been performed to investigate structural and optical properties of $\alpha\text{-ZnP}_2$ and $\beta\text{-ZnP}_2$. In the case of $\beta\text{-ZnP}_2$, we adopted two different initial structures within our study and tested them for significant differences. The first structure is based on the data from Hegyi *et al* [7], hereby named $\beta_1\text{-ZnP}_2$, while the second follows the atomic arrangement observed by Fleet and Mowles [22], and named $\beta_2\text{-ZnP}_2$ (for initial coordinates see tables S9–S11 in the supplementary information available online at stacks.iop.org/JPhysCM/31/265501/mmedia). Combining first principles calculated values with an appropriate selection metric, we assessed the suitability of zinc diphosphides as possible photovoltaic absorber materials and obtained maximum values of 10%.

2. Computational details

Electronic structure calculations based on the density functional theory (DFT) [25, 26] were performed with the projector augmented wave (PAW) [27, 28] pseudo-potential method as implemented in the Vienna *ab initio* simulation package (VASP) [29]. Three different approaches have been considered to describe the exchange-correlation (XC) functional, including the standard Perdew–Burke–Ernzerhof (PBE) general gradient approximation (GGA) [30]; the Hubbard-corrected DFT approach, where an additional potential is added to the GGA total energy to describe the localised (strongly correlated) d -electrons of zinc (GGA+ U) [31] method introduced by Dudarev *et al* [32], with a value of $U_{\text{eff}} = 5$ eV; and the screened hybrid XC functional (HSE06),

where a portion of 25% of the exact non-local Hartree–Fock (HF) exchange is mixed into the PBE total energy [33–35].

The wave function’s kinetic energy cutoff was set to 500 eV (for both zinc diphosphides) together with a Monkhorst–Pack [36] k -mesh of $7 \times 7 \times 3$ (α -ZnP₂) and $5 \times 5 \times 5$ (β -ZnP₂ and β_2 -ZnP₂) to sample the first Brillouin zone. For structural optimisations the change in the total energy and interatomic forces between two steps was required to be less than 10^{-6} eV and 0.01 eV^{-1} , respectively. The optimisation included Van der Waals interactions via the DFT-D3 method developed by Grimme *et al* [37]. Band structure and density of state (DOS) calculations were performed at the optimized structure along high-symmetry directions obtained from the Bilbao Crystallographic Server, using the crystal symmetry data as referenced in table 1 [38–40]. The band structures were plotted using the Wannier90 code [41].

The LOBSTER package, which permits the electronic structure reconstruction through the projection of PAW-based wave functions onto atomic-like basis sets was employed for the chemical-bonding analysis [42, 43]. To obtain the actual projections, local basis functions as given by Bunge were used [44].

In order to study the mechanical properties of the zinc diphosphides, calculations of the elastic constants have been performed within the strain–stress formalism embedded in VASP [45]. The elastic tensor was determined by performing six finite distortions of the lattice and deriving the elastic constants from the strain–stress relationship. Elastic constants, including both the contribution from distortions with rigid ions and the contribution from ionic relaxations, have been calculated. The phonon spectra were calculated using the small-displacement method via the Phonopy code [46]. The plane wave cutoff was increased systematically until convergence up to 2 GPa has been achieved. While exploring the anisotropy properties, we calculated the bulk and the shear modulus using the Voigt–Reuss–Hill approximation [47],

$$K = (K_V \cdot K_R)^{1/2}, \quad (1)$$

$$G = (G_V \cdot G_R)^{1/2}, \quad (2)$$

with

$$K_V = \frac{1}{9} [C_{11} + C_{22} + C_{33} + 2(C_{12} + C_{13} + C_{23})], \quad (3)$$

$$K_R = [S_{11} + S_{22} + S_{33} + 2(S_{12} + S_{13} + S_{23})]^{-1}, \quad (4)$$

$$G_V = \frac{1}{15} [C_{11} + C_{22} + C_{33} - (C_{12} + C_{13} + C_{23}) + 3(C_{44} + C_{55} + C_{66})], \quad (5)$$

$$G_R = 15[4(S_{11} + S_{22} + S_{33}) - 4(S_{12} + S_{13} + S_{23}) + 3(S_{44} + S_{55} + S_{66})]^{-1}. \quad (6)$$

Here, C_{ij} are the elastic constants of zinc diphosphides, S_{ij} elements of the compliance matrix, K_V and K_R denote the upper (Voigt) and lower (Reuss) bound of the effective bulk modulus, K , of the polycrystalline compound, while G_V and G_R represent those for the effective shear modulus, G . In addition,

Table 1. Crystallographic properties of zinc diphosphides.

	α -ZnP ₂	β -ZnP ₂
Crystal structure	Tetragonal	Monoclinic
Space group	$P4_12_12 = D_4^4$ (92) $P4_32_12 = D_4^8$ (96) (Enantiomorphic form [24])	$P2_1/C = C_{2h}^5$ (14)
Class	422	2/m
Pearson symbol	$tP24$	$mP24$

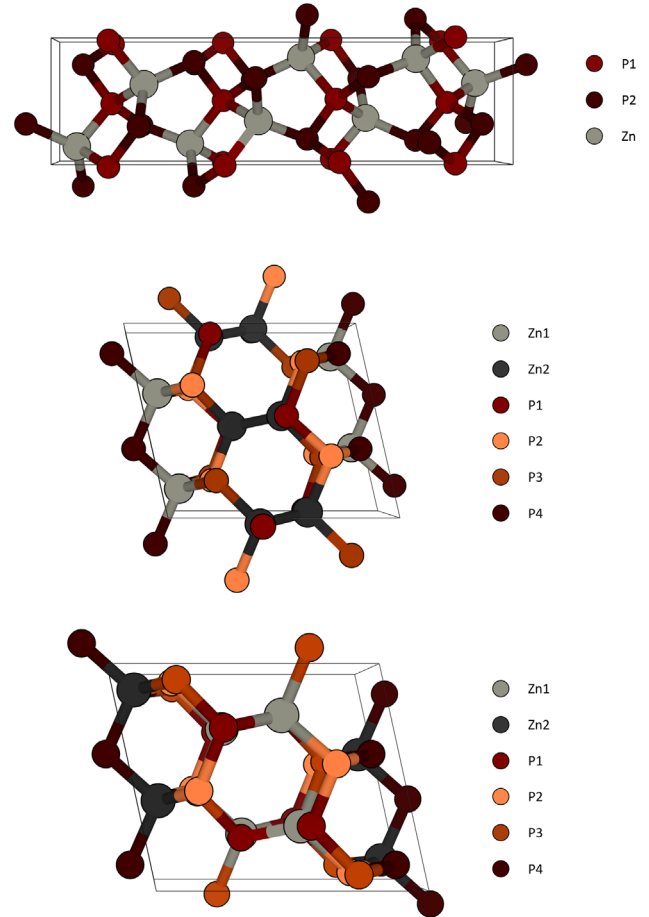


Figure 1. Crystal structures of α -ZnP₂ (top), β_1 -ZnP₂ (middle), and β_2 -ZnP₂ (bottom) together with their corresponding bonding atoms.

the effective Young’s modulus, E , and Poisson’s ratio (ν) can be estimated from the calculated bulk and shear modulus according to the following equations,

$$E = \frac{9KG}{3K + G}, \quad (7)$$

$$\nu = \frac{3K - 2G}{2(3K + G)}. \quad (8)$$

To gain insight into the optical properties of the zinc diphosphides, the frequency-dependent dielectric function $\varepsilon(E) = \varepsilon_1(E) + i\varepsilon_2(E)$ at energy E has been computed in the independent-particle (IP) picture. Local field effects have been neglected and the XC functional has been treated in the

Table 2. Calculated values for lattice constants of zinc diphosphides.

	Lattice constant (Å)		
	α -ZnP ₂	β -ZnP ₂	
Experiment	5.080, 18.590 [52] 5.277, 19.753 [24] 5.073, 18.570 [16]	8.863, 7.288, 7.560 [17]	
Other theory	5.037, 18.316 [18] 5.207, 18.953 [18] 5.097, 18.625 [19] 5.098, 18.604 [20]	8.884, 7.322, 7.606 [20]	
This work	α -ZnP ₂	β_1 -ZnP ₂	β_2 -ZnP ₂
GGA	5.047, 18.412	8.552, 7.274, 7.552	8.611, 7.239, 7.530
GGA+U	5.032, 18.357	8.522, 7.265, 7.539	8.592, 7.227, 7.518

GGA and HSE06 approximation. From the dielectric function, we have calculated the absorption coefficient α

$$\alpha(E) = \frac{4\pi E}{hc} k(E), \quad (9)$$

where h is Planck's constant, c the speed of light, and $k(E)$ the extinction coefficient,

$$k(E) = \left(\frac{|\varepsilon(E)| - \varepsilon_1(E)}{2} \right)^{\frac{1}{2}}. \quad (10)$$

Also, to assess the solar-absorbing potential of zinc diphosphides, the 'spectroscopic limited maximum efficiency' (SLME) has been computed. This concept, proposed by Yu and Zunger [48], offers a calculable selection metric to scan materials based on their band gap energies, shape of absorption spectra, and non-radiative recombination losses. It expands the traditional Shockley–Queisser (SQ) limit to capture underpinning mechanisms that show relevance to real-time applications.

Spin–orbit coupling (almost negligible experimental value [49]) and excitonic effects have not been included in this work.

3. Results and discussion

3.1. Structural properties

The optimised crystal structures of α -, β_1 -, and β_2 -ZnP₂ are shown in figure 1, whereas the calculated lattice parameters in comparison with experimental and earlier theoretical results are summarised in table 2.

In general, we found good agreement between our calculated unit cell parameters and those reported in literature. A small but not insignificant difference between lattice constants of β_1 -ZnP₂ and β_2 -ZnP₂ was noticed, with β_2 -ZnP₂ being somewhat closer to the experimental data. None of the studied compounds showed magnetic ground state properties. Obtained values of bonds and angles for all three structures are listed in tables S1–S6 (these can be found in the supplementary information file).

Within α -ZnP₂ (figure 1—top), there are three crystallographically independent atoms (Zn, P₁, and P₂) with each zinc

Table 3. Calculated values for the bulk modulus B (GPa), shear modulus G (GPa) Young's modulus E (GPa) and Poisson's ratio ν , together with previous experimental and theoretical results.

		α -ZnP ₂	β_1 -ZnP ₂	β_2 -ZnP ₂
Bulk modulus—VRH (GPa)	GGA	76.83	65.85	75.06
	Experiment			
	Theory			
Bulk modulus—EOS (GPa)	GGA	76.56	64.17	73.84
	Experiment	62.91 [18]	64.5 [13]	
	Theory	98.84 [18], 63.13 [18], 73.34 [19], 72 [20]	68 [20]	
Shear modulus (GPa)	GGA	67.01	50.53	70.97
	Experiment	35.7 [13], 39.3 [13]	17.97 [13]	
	Other theory	44 [20]	44 [20]	
Young modulus (GPa)	GGA	155.74	120.72	161.89
	Experiment	79.95 [13]	42.97 [13]	
	Theory	110 [20]	110 [20]	
Isotropic Poisson ratio	GGA	0.162	0.194	0.141
	Experiment	0.12 [13], 0.371 [13]	0.217 [13], 0.479 [13]	
	Theory	0.24 [20]	0.23 [20]	

atom being bonded to four P atoms (two of each, P₁ and P₂), whereas each phosphorus atom has two bonds with Zn and two with P atoms of the other crystallographic type. The overall arrangement gives four phosphorus chains per unit cell parallel to either a or b lattice vector, with possible chain formations in the c direction being disrupted by zinc atoms. When projected in the a or b direction (bc and ac planes), chains resemble tetragonally shaped wells. Every zinc interacts with three chains (two running in a direction and one in b or vice versa) through four Zn–P bonds building a network of pentagons alternating with existing P chain wells. The P–P bonds of all chains are 2.17 and 2.21 Å, and match distances in pure black phosphorus [50]. The average Zn–P bond length is 2.37 Å, which is shorter than the distance calculated from Pauling's tetrahedral radii, 2.41 Å [51]. The biggest deviation from the ideal tetrahedral angle (109.5°) comes from a Zn bonded to

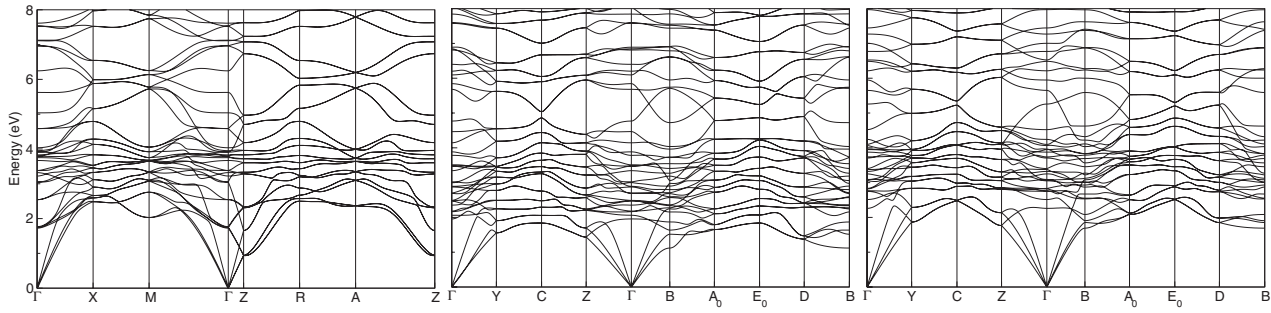


Figure 2. Calculated phonon dispersion curves of α -ZnP₂ (left), β_1 -ZnP₂ (middle), and β_2 -ZnP₂ (right) along high-symmetry points of the Brillouin zone using PBE.

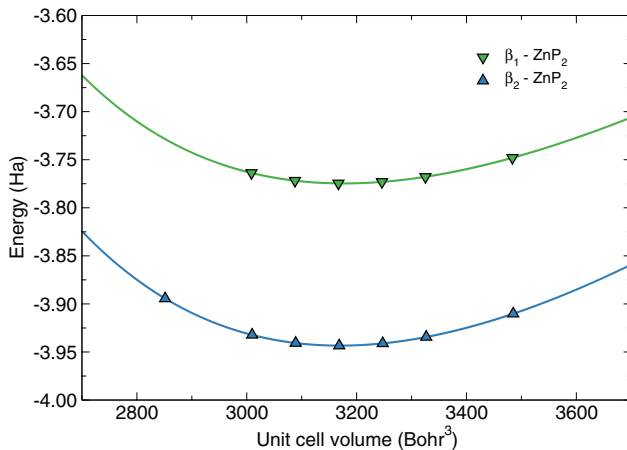


Figure 3. Calculated energy versus volume data points for β_1 -ZnP₂ and β_2 -ZnP₂ using PBE together with the fitted values obtained from the Birch–Murnaghan EOS.

two P₂ atoms (124.3°) and is a direct consequence of the 0.05 Å difference in the bond length. Furthermore, bond lengths shorter than covalent ones indicate fractional ionic character and increase in the bond strength and could therefore lead to an opening of the band gap.

Compared to the α -ZnP₂ phase, two modifications of the monoclinic β -ZnP₂ phase can be distinguished, which are denoted in this study as β_1 -ZnP₂ and β_2 -ZnP₂ based on the presence or absence of zinc–zinc bonds in the structure.

For β_1 -ZnP₂ (figure 1 middle), unlike α -ZnP₂, six crystallographically independent atoms can be identified in the unit cell: Zn₁, Zn₂, P₁, P₂, P₃, and P₄. Zn₁ is bonded to four P atoms as expected ($2 \times P_1, P_2, P_3$), with P₂, P₃, and P₄ atoms having two bonds with zinc and two bonds with phosphorus atoms. Both Zn₂ and P₁ are, however, surrounded by one Zn₂ and three independent phosphorus atoms (P₂, P₃, P₄). The final structure has only one P chain per unit cell which changes path along all three directions. P–P distances alternate from 2.19 Å to 2.26 Å, and even to 2.32 Å, causing Zn–P bonds and angles to vary over a wider range than in the tetragonal structure. Zn–Zn bonds are in the plane perpendicular to the *c* axis and tilted by 56.673° from the *b* axis which agrees well with experimental studies ($\pm 57^\circ$) [7]. The distance between bonded zinc atoms is very short compared to the covalent radius of the zinc atom,

but it is not the first time this has been noticed [53]. According to the structural parameters, it could also be said that the Zn₂ atom resembles Zn in α -ZnP₂, followed by P₁ and P₄ atoms behaving like P₁ and P₂ in the α -modification. Moreover, the presence of the metallic bonds may result in the delocalization of electrons and a decrease of the band gap.

The β_2 -ZnP₂ phase (figure 1 bottom) does not possess zinc atoms bonded to each other, but it still has six crystallographically independent atoms (Zn₁, Zn₂, P₁, P₂, P₃, and P₄). The different types of Zn atoms arise from their positions—half of the atoms sit inside phosphorus chains, while the other half is in between the two chains. Therefore, all zinc atoms are binding four phosphorus atoms, and all phosphorus atoms have two bonds with zinc and two bonds with P atoms of a different type, similar to α -ZnP₂. There are two phosphorus chains per unit cell and their projection is in the shape of an open irregular pentagon. Most angles are closer to the perfect tetrahedral angle compared to β_1 -ZnP₂, leading to better stability. Comparison of the angles of β_2 -ZnP₂ with α -ZnP₂ reveals analogues in the two structures: the tetragon surrounding Zn₁ closely resembles the tetragon of Zn from α -ZnP₂, while P₁ and P₄ tetragons have their twins in P₁ and P₂, respectively. Despite these similarities, three additional crystallographic species in the β_2 -ZnP₂ phase disrupt the formation of the same structural patterns as in α -ZnP₂. Longer Zn–P bonds indicate less ionic character and lower band gap values.

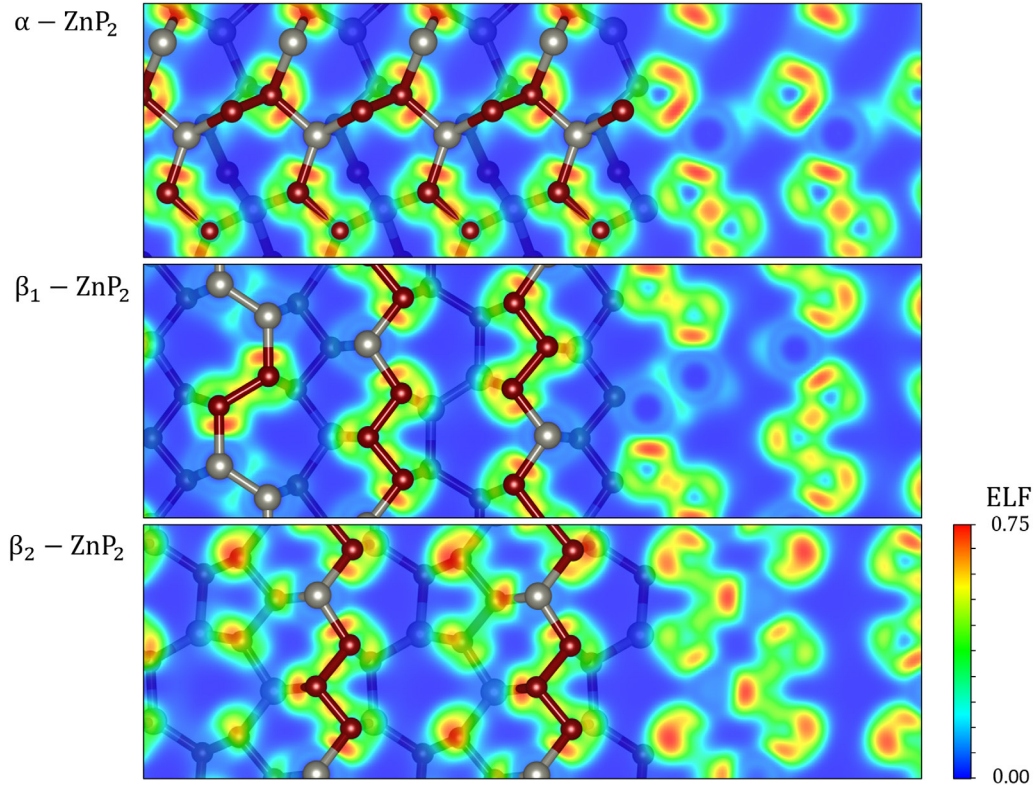
In both the tetragonal and monoclinic phases, all atoms are tetrahedrally coordinated with Zn–P and P–P bonds within the same tetrahedron differing by $\sim 2\%$ – 3% . These differences account for deviations in ideal tetrahedral angles and lead to tetrahedra being somehow distorted when forming a continuous structure. Variations in bond lengths and angle distortions between the two phases provide an insight in the ionic share of bonding and can serve as a guide for the expected electronic structures.

3.2. Elastic properties and lattice dynamics

To obtain information about the mechanical stabilities of the zinc diphosphides, the elastic stiffness constants were calculated. For tetragonal and monoclinic structures, there are six

Table 4. Bader charge analysis of zinc diphosphides.

	Bader charge (e^-)					
	Zn ₁	Zn ₂	P ₁	P ₂	P ₃	P ₄
α -ZnP ₂		0.7071	−0.3531	−0.3543		
β_1 -ZnP ₂	0.7139	0.3669	−0.0976	−0.2956	−0.3075	−0.3758
β_2 -ZnP ₂	0.7006	0.7014	−0.3716	−0.3318	−0.3484	−0.3502

**Figure 4.** Electron localization function (ELF) for considered three zinc diphosphides calculated using hybrid DFT.

and thirteen independent elastic constants, respectively. The calculated elastic constants, together with available experimental and theoretical data are given in tables S7 and S8 (supplementary information). As shown in these tables, both zinc diphosphide phases satisfy the mechanical stability criteria by Cowley [54]. Elastic constants obtained from DFT are usually based on single-crystal zinc diphosphides, while the Voigt–Reuss–Hill approximation (VHR) can induce the elastic properties of polycrystalline compounds. Equations for the calculated bulk modulus (B), shear modulus (G), and Young’s modulus (E) in the VHR approximation can be found in the literature [55]. B measures the resistance of material to volume change, G the resistance to shape change, while E often gives a measure of the stiffness of the solid.

Calculated values of B , G , and E for zinc diphosphides, shown in table 3, vary only slightly from each other, indicating that the three compounds have almost identical resistance to external mechanical forces. The Poisson’s ratio allows us to test the ductility/brittleness of material. A material is characterised as ductile if $G/B < 0.5$, otherwise it is classed as brittle. According to this criterion, α -ZnP₂, β_1 -ZnP₂, and β_2 -ZnP₂ are all ductile materials.

Most materials undergo phase transitions driven by lattice instability, both those induced by pressure and those induced by temperature. This instability can be an elastic one (leading to a change of the unit cell shape) or a phonon instability (a so-called *soft phonon*, whose energy goes to zero) [56]. For a material to be stable, it needs to satisfy a set of conditions [57]. One of the stability requirements of a crystal lattice is its invariability towards any small displacements of atoms. This condition equals to the statement of all phonon frequencies possessing positive values. The identified soft phonon mode appears whilst an external parameter is changed, leading to a crystal instability, resulting with a new crystal structure.

Calculated full phonon dispersion curves along high-symmetry lines in the Brillouin zone are depicted in figure 2. All three studied zinc diphosphide compounds are dynamically stable at atmospheric pressure, since there is no occurrence of imaginary frequencies. The result for β_1 -ZnP₂ is somewhat surprising considering the fact that it was evaluated as misinterpreted structural data, and it indicates that β_1 -ZnP₂ might be present in real monoclinic crystals as an impurity and future experimental and theoretical studies should not rule it out *a priori*.

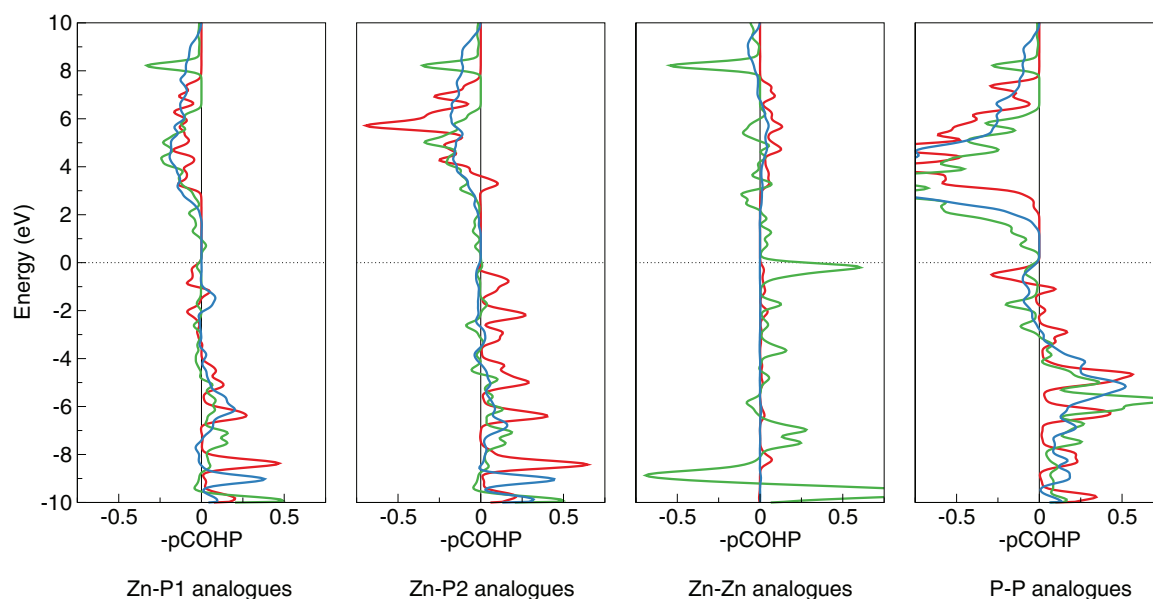


Figure 5. Projected crystal orbital Hamilton populations (pCOHPs) for analogues bonds between the tetragonal and monoclinic phases of zinc diphosphide. The energy axis is shown relative to the Fermi level. Bonding states are indicated with positive, while anti-bonding states are indicated with negative values on the x -axis ($-p\text{COHP}$).

Table 5. Calculated electronic band gap energies for all three zinc diphosphides in comparison to other theoretical calculations and experiments. Literature does not distinguish between the two monoclinic phases, so their values are presented together.

Electronic band gap energies (eV)				
	$\alpha\text{-ZnP}_2$		$\beta\text{-ZnP}_2$	
	Direct	Indirect	Direct	
Experiment	2.455 [58]	2.10 [16] 2.207 [58] 2.25 [12] 2.30 [17]	1.33 [12] 1.44–1.60 [4, 59–60]	
Other theory	1.54 [18] 1.91 [18]	1.48 [20] 1.58 [24]	0.78 [20]	
This work	$\alpha\text{-ZnP}_2$		$\beta_1\text{-ZnP}_2$	$\beta_2\text{-ZnP}_2$
	Direct	Indirect	Indirect	Direct
GGA	1.53 (Γ)	1.40 ($M - \Gamma$)	—	0.76 (Γ)
GGA+U	1.50 (Γ)	1.36 ($M - \Gamma$)	—	0.78 (Γ)
HSE06	2.26 (Γ)	2.13 ($M - \Gamma$)	0.04 ($E_0 - B$)	1.46 (Γ)

To distinguish further between the stability of the monoclinic $\beta_1\text{-ZnP}_2$, and $\beta_2\text{-ZnP}_2$ structures, the equilibrium properties were calculated by fitting the computed total energy versus volume curve with the Birch–Murnaghan equation of state (EOS), which shows the $\beta_2\text{-ZnP}_2$ structure to be thermodynamically more stable (figure 3).

3.3. Charge analysis

Following the general trend of shorter bonds having a higher share of ionic character, $\beta_1\text{-ZnP}_2$ with average Zn–P bond length of ~ 2.35 Å would be expected to have the most pronounced ionic nature. However, this effect could be

compensated for long P–P and metallic Zn–Zn bonds, which dominate the whole structure. All Zn–P bonds in $\alpha\text{-ZnP}_2$ are shorter than pure covalent ones between these species, indicating partial ionic nature. For $\beta_2\text{-ZnP}_2$ this is true only for 50% of the Zn–P bonds with the remaining bonds either being the length of the perfect covalent bond or longer, indicating less ionic character compared to $\alpha\text{-ZnP}_2$. To confirm those indications, charge analysis calculations have been performed and the results are shown in table 4. The calculated charge density difference for $\alpha\text{-ZnP}_2$ shows a shift of bonding electrons towards P atoms as a result of the ionic character, with corresponding Bader charges of $-0.35 e^-$ for P and $0.71 e^-$ for Zn. The metallic zinc–zinc bonds in $\beta_1\text{-ZnP}_2$ cause the delocalisation of electrons. Consequently, electrons of P₁ atoms tend to migrate in delocalised clouds, leaving one fourth of phosphorus atoms with charge of only $-0.10 e^-$ and bonded zinc atoms with reduced positive charge of $0.37 e^-$. Interestingly, in the case of $\beta_2\text{-ZnP}_2$ only minor differences in charge are obtained compared to the α -phase ($0.70 e^-$ for Zn and -0.33 , -0.34 , -0.35 , and $-0.37 e^-$ for P atoms).

In figure 4, the electron localisation function (ELF) as a direct space depiction of the electron distribution has been plotted for all three zinc diphosphide phases to indicate the extent of the spatial localisation of reference electrons. With values close to 0 (blue) corresponding to vacuum, moderate values (green) to uniform electron gas, and values closest to 0.75 (red) resembling the perfect localisation, a higher ELF value at a considered point indicates higher localisation of electrons in that area compared to a uniform electron gas of the same density. It is evident that the electrons are localised around phosphorus atoms with P atoms in $\alpha\text{-ZnP}_2$ having the most prominent localisation. These results imply higher ionic features of the Zn–P interaction in the α -phase compared to the Zn–P interactions in the $\beta\text{-ZnP}_2$ phases, which can lead

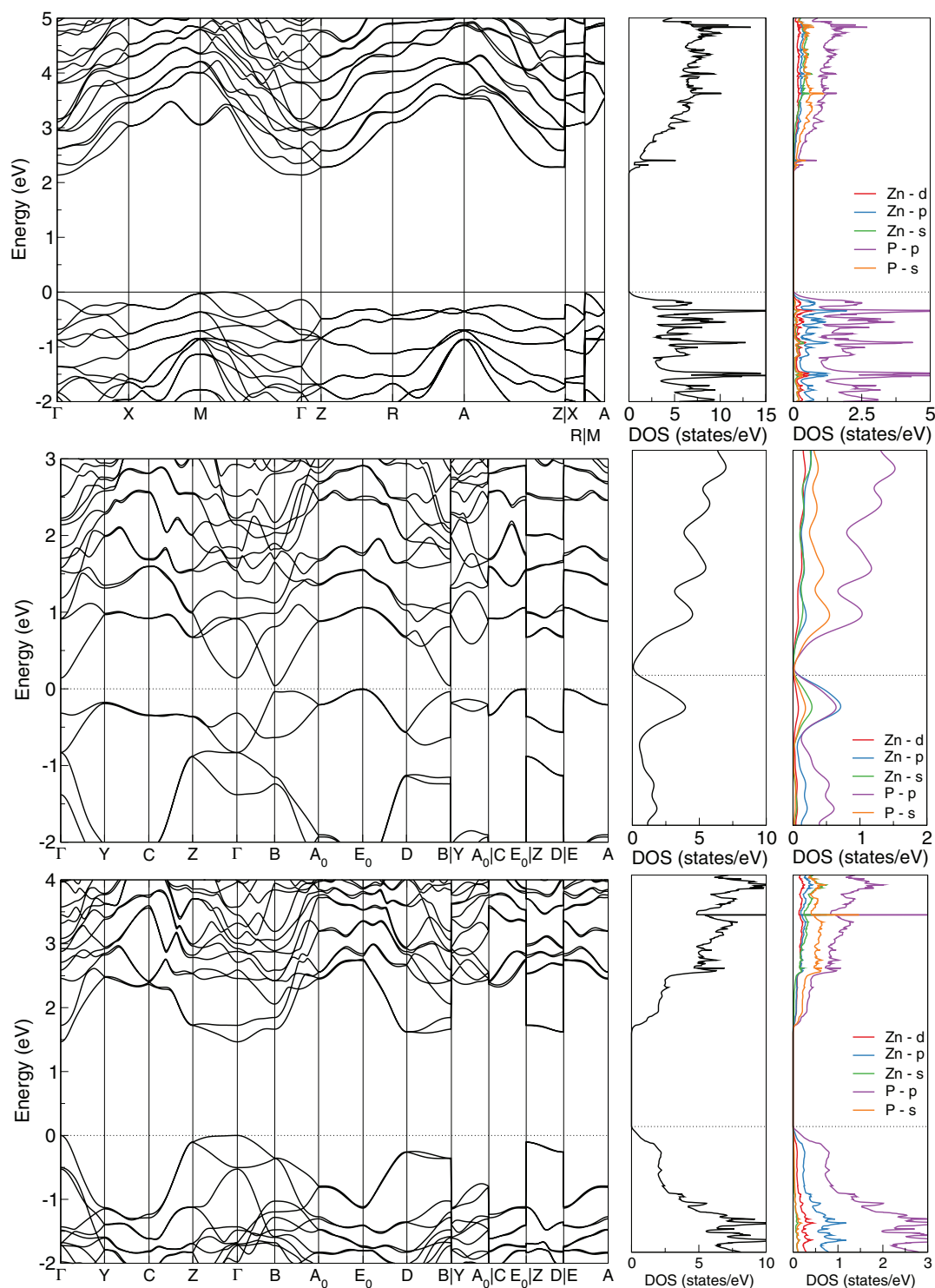


Figure 6. Calculated band structure of α -ZnP₂, β_1 -ZnP₂, and β_2 -ZnP₂ (left hand side, from top to bottom) together with the total (middle) and projected (right) densities of states using HSE06 calculations. The valence band maximum is set to zero.

to increased band gap values. Cyan areas between zinc atoms denote delocalised electrons of the metallic bond and exist only for β_1 -ZnP₂.

Since the total charge for single atoms includes electrons from four bonds, not much can be concluded about the nature and strength of each bond. Direct bond analysis can, however, reveal important information and has therefore been

conducted through the crystal orbital Hamiltonian population (COHP) technique. COHP data allow comparison between bonds of analogous atoms in each structure and do not rely on any other parameter. Projected COHP (pCOHP) for matching Zn–P, Zn–Zn, and P–P bonds are shown in figure 5. Although bonding peaks for Zn–P analogues appear at different energy ranges, the similarity in the shapes of the pCOHP curves reveals

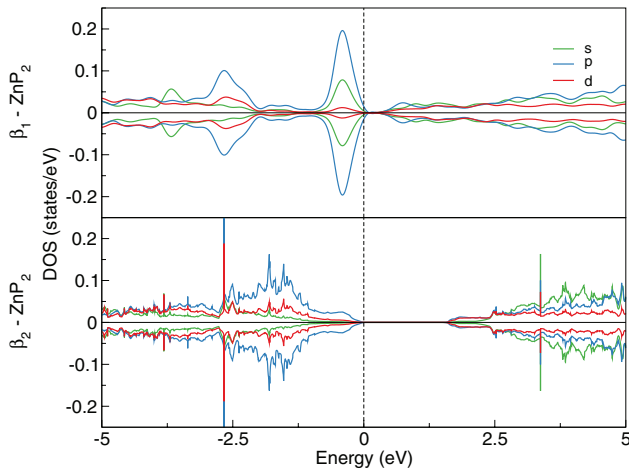


Figure 7. Projected densities of state for analogue Zn atoms in β_1 -ZnP₂ and β_2 -ZnP₂.

the resemblance of the Zn–P bonds in the three zinc diphosphides. The highest peak at ~ -8 eV indicates the strongest bond amongst the three phases and belongs to α -ZnP₂. In the case of Zn–Zn bonds, α -ZnP₂ and β_2 -ZnP₂ do not show any bonding states, while the Zn–Zn bond appears to be more than double the strength of Zn–P bonds in β_1 -ZnP₂. All P–P bonds are similar with differences arising mostly from discrepancies in length.

3.4. Electronic properties

The electronic band structures, total densities of state (DOS), and projected densities of state (pDOS) for α -ZnP₂, β_1 -ZnP₂, and β_2 -ZnP₂ were calculated using standard GGA, Hubbard-corrected GGA+*U*, and screened hybrid DFT approaches and are summarised in table 5.

Overall, our calculated results are consistent with experimental data and earlier DFT predictions. Although the standard GGA functional captures accurately the indirect nature, the obtained band gap value of α -ZnP₂ is ~ 0.70 eV smaller than the experimentally determined one. Introducing an additional on-site potential ($+U_{\text{eff}}$) to GGA increases the band gap for most common semiconductors. With α -ZnP₂ this is not the case, as a counterintuitive shrinking of the band gap value in comparison with the pure GGA one was observed (for ~ 0.05 eV). A close examination of the calculated densities of states clarified this behaviour. The applied potential localizes the *d* orbitals of zinc atoms thereby lowering their energy level by ~ 1 eV, as has been depicted in figure S4. Because the top of the valence band consists mostly of phosphorus *p* orbitals, inducing (or increasing) the $+U_{\text{eff}}$ value does not influence the value of the band gap.

Adding a fraction of the short-range screened exchange parameter (HSE06 functional, $\alpha = 0.25$) to the GGA-PBE functional resulted in opening of the band gap, where α -ZnP₂ now has an indirect band gap of 2.13 eV, which is in a very good agreement with experimental data. The calculated band structure along high-symmetry directions together with the accompanying DOS and pDOS of α -ZnP₂

obtained by the hybrid functionals are shown in figure 6. The bottom of the conduction band is located at the Γ point, while the top of the valence band can be found along the $M - \Gamma$ path. Analysis of the orbital pDOS reveals that the majority of carriers at the top of the valence band originate from P-*p* orbitals with a small contribution from Zn-*s* and Zn-*d* states, whereas the bottom of the conduction band mainly arises from P-*s* states.

The band structures and DOS results of β_1 -ZnP₂ and β_2 -ZnP₂ extend the proposed mechanisms obtained from the corresponding charge analysis (shown in figure 6). Results derived from the GGA functional identified β_1 -ZnP₂ as a pure metal, without any bands separated by a gap. Hybrid functionals, on the other side, indicate a small band gap value which was tentatively assigned as an artefact of the calculation itself, rather than an intrinsic property. DOS calculations have shown how the top of the valence band arises from equally contributing Zn-*p*, Zn-*s* and P-*p* orbitals, which contrasts with α -ZnP₂ where Zn states play a minor role. The bottom of the conduction band originates from P-*p* and P-*s* states, similar to the tetragonal phase. As proposed, high Zn-*p* and Zn-*s* states originating from the highly metallic character of Zn–Zn bonds prevent the material from showing semiconducting properties, which is shown in figure 7.

This metallic character is in contrast with β_2 -ZnP₂, which already showed a direct band gap from GGA calculations, located at the highly symmetric Γ point, although with a value underestimating experimental ones for ~ 0.80 eV. Employing of hybrid functionals gives a direct first transition between valence and conduction band with a corrected value of 1.46 eV, which is in very good agreement with available experimental data. Similar to α -ZnP₂, the top of the valence has been linked with majority states originating from P-*p* orbitals, leaving Zn-*d* orbitals with only a minor influence.

Overall, there is a strong overlap between the zinc and the phosphorus components of the DOS structures over the whole range of energies, which confirms the formation of covalent bonds between the two species and a low level of ionicity.

Moreover, it is noted how previous theoretical studies have failed to include all relevant high-symmetry points in the first Brillouin zone. The multivalley nature of the band structure of zinc diphosphides can easily lead to band gap values which do not correspond to the global lowest transitions.

3.5. Optical properties and SLME

The optical properties of semiconducting materials are inherently linked to their electronic and vibrational properties. An understanding of how macroscopic properties can be linked to microscopic parameters is important in many applications, especially photovoltaics. At a microscopic level in bulk materials, the complex dielectric function is closely connected with the band structure. The dielectric function generally describes the reaction of a system to an external force. As long as the reaction is linear, the linear response functions (describing the reaction) are properties of the system itself, rather than being force dependent. This concept then can be

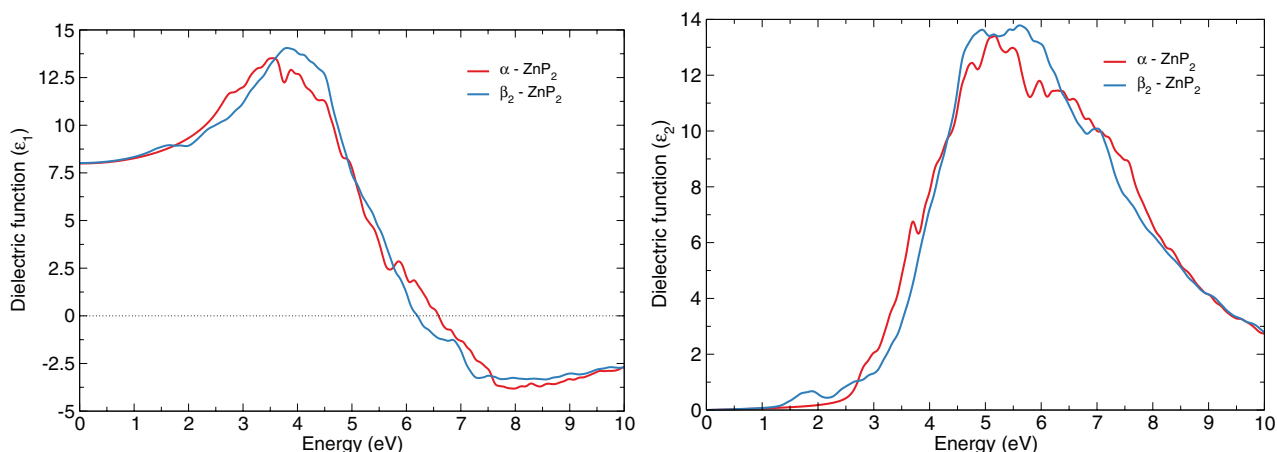


Figure 8. Calculated real part of the dielectric function (ϵ_1 , left) and imaginary part of the dielectric function (ϵ_2 , right) for α -ZnP₂ and β_2 -ZnP₂ employing the HSE06 functional. Values have been averaged over three cartesian coordinates.

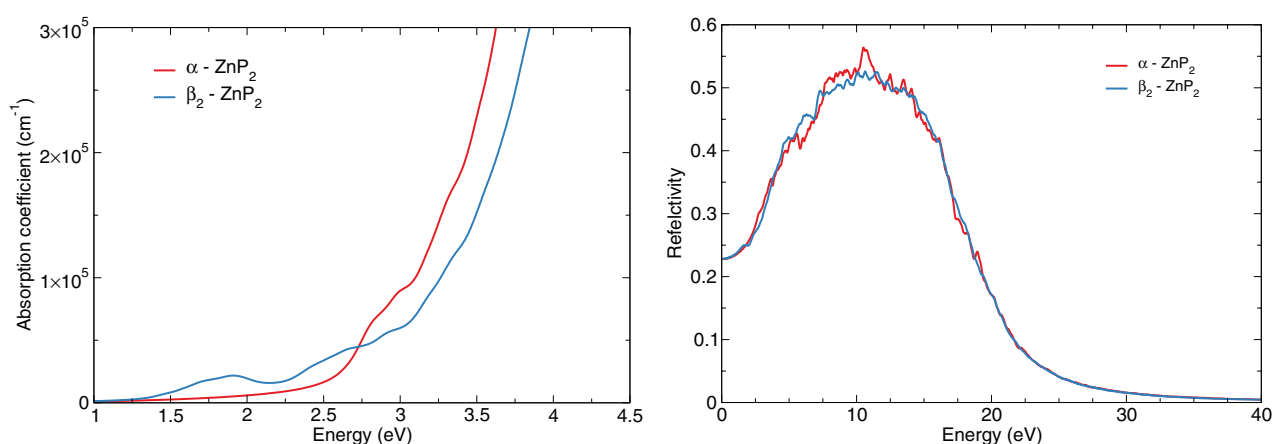


Figure 9. Calculated absorption coefficient (left) and reflectivity (right) using the HSE06 functional for α -ZnP₂ and β_2 -ZnP₂ averaged over cartesian coordinates.

applied to the whole electromagnetic spectrum whilst studying complex materials [61].

The calculated real (dispersive, ϵ_1) and imaginary (absorptive, ϵ_2) parts of the dielectric function for α -ZnP₂ and β_2 -ZnP₂ are shown in figure 8. The monoclinic phase β_1 -ZnP₂ has been omitted from the optical analysis due to its pronounced metallic character, which makes the compound less attractive as a potential PV absorber. The calculated absorption coefficient, an ingredient needed for the PCE analysis, together with the material's reflectivity has been calculated and shown in figure 9.

The value of the static dielectric function $\epsilon_1(0)$ is equal to 7.993 for α -ZnP₂ and 8.017 for β_2 -ZnP₂, which corresponds well with previous experimental results yielding values in the range 9–14 for temperatures between 78–100 K [59]. Within the imaginary part of the dielectric function, in principle, one can associate certain peaks with transitions in the band structure.

For α -ZnP₂, the absorption onset is noted around an energy of 2 eV, which corresponds to the calculated fundamental band transition between the top of the valence and bottom of the conduction band. However, the aforementioned transition is indirect in nature and forbidden by symmetry. This corresponds to a vanishing electronic dipole transition matrix element resulting in a weaker response of the system to incoming

electromagnetic radiation. The first significant peak that can be observed lies around 3 eV and arises from transitions deeper within the band structure. Most of the transitions up to that point are still forbidden by symmetry and contribute only weakly to the response functions. On the other hand, β_2 -ZnP₂ has a direct allowed transition between the bands separated by an electronic gap. This transition takes place around 1.5 eV, as one would expect from the calculated band gap value. By looking at the probabilities of absorbing photons of a certain wavelength, which is depicted in figure 9, one can clearly observe the earlier absorption onset for β_2 -ZnP₂ compared to α -ZnP₂.

After calculation of the band structures and dielectric function of the zinc diphosphides, we have obtained all the required information to assess their photovoltaic potential. The calculated SLME as a function of the film thickness for zinc diphosphides was calculated and shown in figure 10. For a reasonable reference thickness of 0.5 μ m we obtained 0.28% and 9.39% efficiencies for α -ZnP₂ and β_2 -ZnP₂, respectively. The origin of this somewhat surprising difference comes from the distinct band nature of the two compounds. For α -ZnP₂, there is a non-zero difference between the direct allowed and fundamental band transition ($\Delta = E_g^{\text{DA}} - E_g > 0$) which indicates that non-radiative processes are significant within this compound.

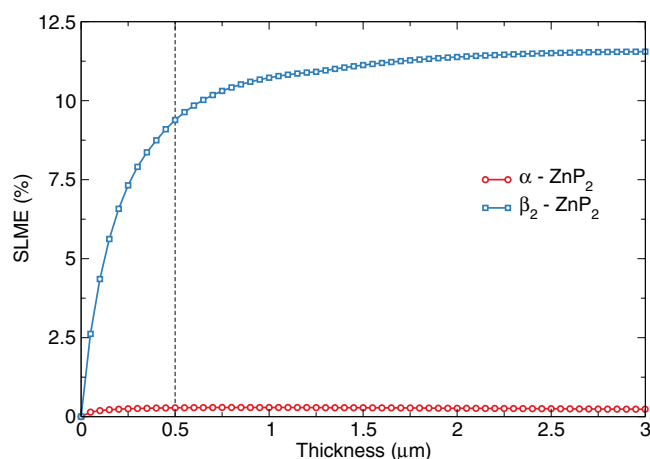


Figure 10. Calculated spectroscopic limited maximum efficiency (SLME) for α -ZnP₂ and β_2 -ZnP₂ plotted as a function of the film thickness.

Although the SLME metric was found to overestimate the reverse saturation current, in our case it is of the order of 10^{-5} , which seems to be a reasonable value compared to other similar classes of materials [62]. If we would consider radiative recombination as the only process taking place, we would resemble the classic SQ limit and obtain an efficiency value of 5.86% for α -ZnP₂ (considering a 0.5 μm thick absorber). However, the fundamental transition for β_2 -ZnP₂ is already dipole allowed and we can expect radiative recombination as the main recombination process governing absorption.

4. Conclusion

A comprehensive computational study of the structures and properties zinc diphosphides has been undertaken. Calculations employing the HSE06 XC functional have been proven accurate in describing structural, mechanical, electronic, and optical properties of all three targeted zinc diphosphide compounds. Unlike the stable tetragonal phase, the two monoclinic structures show different stabilities and bonding character. Specific Zn–Zn bonds within β_1 -ZnP₂ cause metallic behaviour and a lower stability than β_2 -ZnP₂. Moreover, electronic structure calculations that reproduce the experimentally observed features have been conducted. They show diverse band transitions and electric dipole moments which lead to substantially different optical properties. In addition, we assessed the thin-film photovoltaic potential of zinc diphosphides, showing β_2 -ZnP₂ as a promising absorbing material. Future investigations will expand the work presented here to include the effect of doping, or the creation of heterojunctions on tuning the electronic and optical properties of zinc diphosphides to achieve efficient charge carrier separation and improved photovoltaic efficiencies.

Acknowledgments

N Y D acknowledges the UK Engineering and Physical Sciences Research Council (EPSRC) for funding (Grant No. EP/S001395/1). A Ž acknowledges the Cardiff University School

of Chemistry for a PhD studentship. NHdL also acknowledges the UK EPSRC for funding (Grant No. EP/R512618/1). This work was performed using the computational facilities of the Centre for High Performance Computing in Cape Town (CHPC). This work has also used the computational facilities of the Advanced Research Computing at Cardiff (ARCCA) Division, Cardiff University, and HPC Wales. Information on the data that underpins the results presented here, including how to access them, can be found in the Cardiff University data catalogue at <https://doi.org/10.17035/d.2018.0054381131>.

ORCID iDs

Aleksandar Živković  <https://orcid.org/0000-0003-1347-6203>

Nelson Y Dzade  <https://orcid.org/0000-0001-7733-9473>

References

- [1] Bernardi M and Grossman J C 2016 Computer calculations across time and length scales in photovoltaic solar cells *Energy Environ. Sci.* **9** 2197–218
- [2] Zdanowicz W and Zdanowicz L 1975 Semiconducting compounds of the A^{II}B^V group *Annu. Rev. Mater. Sci.* **5** 301–28
- [3] Rubenstein M and Dean P J 1970 Preparation of zinc diphosphides and the low-temperature luminescence and absorption of the tetragonal polymorph *J. Appl. Phys.* **41** 1777–86
- [4] Sobolev V V and Syrbu N N 1972 Optical spectra and energy band structure of the monoclinic crystals ZnP₂ and ZnAs₂ *Phys. Status Solidi* **51** 863–72
- [5] Fagen E A 1979 Optical properties of Zn₃P₂ *J. Appl. Phys.* **50** 6505–15
- [6] Sobolev V V and Syrbu N N 1974 Optical properties and energy band structure of Zn₃P₂ and Cd₃P₂ crystals *Phys. Status Solidi* **64** 423–9
- [7] Hegyi I J, Loebner E E, Poor E W and White J G 1963 Two crystal forms of ZnP₂, their preparation, structure, and optoelectronic properties *J. Phys. Chem. Solids* **24** 333–7
- [8] Ito K, Matsuura Y, Nakazawa T and Takenouchi H 1981 Photovoltaic effect in monoclinic ZnP₂ *Japan. J. Appl. Phys.* **20** 109
- [9] Stackelberg M V and Paulus R 1935 Untersuchungen an den Phosphiden und Arseniden des Zinks und Cadmiums. Das Zn₃P₂-gitter *Z. Phys. Chem.* **28B** 427
- [10] White J G 1965 The crystal structure of the tetragonal modification of ZnP₂ *Acta Crystallogr.* **18** 217–20
- [11] Manolikas C, van Tendeloo J and Amelinckx S 1986 The ‘devil’s staircase’ in CdP₂ and ZnP₂ *Phys. Status Solidi* **97** 87–102
- [12] Zanin I E, Aleinikova K B and Antipin M Y 2003 Analysis of chemical bonding in the α and β modifications of zinc diphosphide from x-ray diffraction data *Crystallogr. Rep.* **48** 199–204
- [13] Soshnikov L E, Trukhan V M, Haliakevich T V and Soshnikova H L 2005 Dielectric and elastic properties of CdP₂, ZnP₂ and ZnAs₂ single crystals *Mold. J. Phys. Sci.* **4** 201–11
- [14] Sobolev V V, Kozlov A I, Polygalov Y I, Tupitsyn V E and Poplavnoi A S 1989 Reflectivity spectra and band structure of the zinc and cadmium diphosphides *Phys. Status Solidi* **154** 377–88

- [15] Jayaraman A, Maines R G and Chattopadhyay T 1986 Effect of high pressure on the vibrational modes and the energy gap of ZnP_2 *Pramana J. Phys.* **27** 291–7
- [16] Bodnar I V, Rud V Y, Rud Y V, Vaipolin A A, Osipova M A and Ushakova T N 2009 Photosensitive structure from the tetragonal modification of ZnP_2 single crystals *J. Appl. Spectrosc.* **76** 220–6
- [17] Aleynikova K B, Kozlov A, Kozlova S G and Sobolev V 2004 Crystal chemistry and optical properties of monoclinic zinc diphosphide *Mold. J. Phys. Sci.* **3** 137–48
- [18] Fan C-L, Cheng X-L and Zhang H 2009 First-principles study of the structural and electronic properties of the α modification of zinc diphosphide *Phys. Status Solidi* **246** 77–81
- [19] Yang Z, Wang X, Liu L, Yang S and Su X 2011 Density functional theory studies on elastic and electronic properties of tetragonal ZnP_2 *Solid State Sci.* **13** 1604–7
- [20] Huang H M, Li Y L and Zeng Z 2013 Structural, elastic, and electronic properties of compressed ZnP_2 *Physica B* **419** 112–5
- [21] Fleet M E 1974 The crystal structure of ZnAs_2 *Acta Crystallogr. B* **30** 122–6
- [22] Fleet M E and Mowles T A 1984 Structure of monoclinic black zinc diphosphide, ZnP_2 *Acta Crystallogr. C* **40** 1778–9
- [23] Gorban I S, Bilyi M M, Dmitruk I M and Yeshchenko O A 1998 Multiserial structure of excitonic energy spectrum in monoclinic ZnP_2 crystal *Phys. Status Solidi* **207** 171–81
- [24] Aleinikova K B, Kozlov A I, Kozlova S G and Sobolev V V 2002 Electronic and crystal structures of isomorphous ZnP_2 and CdP_2 *Phys. Solid State* **44** 1257–62
- [25] Kohn W and Sham L J 1965 Self-consistent equations including exchange and correlation effects *Phys. Rev.* **140** A1133
- [26] Hohenberg P and Kohn W 1964 Inhomogeneous electron gas *Phys. Rev.* **136** B864–71
- [27] Blöchl P E 1994 Projector augmented-wave method *Phys. Rev. B* **50** 17953–79
- [28] Kresse G and Joubert D 1999 From ultrasoft pseudopotentials to the projector augmented-wave method *Phys. Rev. B* **59** 1758–75
- [29] Kresse G and Furthmüller J 1996 Efficient iterative schemes for *ab initio* total-energy calculations using a plane-wave basis set *Phys. Rev. B* **54** 11169–86
- [30] Perdew J P, Burke K and Ernzerhof M 1996 Generalized gradient approximation made simple *Phys. Rev. Lett.* **77** 3865–8
- [31] Anisimov V I, Zaanen J and Andersen O K 1991 Band theory and Mott insulators: Hubbard U instead of Stoner I *Phys. Rev. B* **44** 943–54
- [32] Dudarev S L, Botton G A, Savrasov S Y, Humphreys C J and Sutton A P 1998 Electron-energy-loss spectra and the structural stability of nickel oxide: an LSDA+U study *Phys. Rev. B* **57** 1505–9
- [33] Heyd J, Scuseria G E and Ernzerhof M 2003 Hybrid functionals based on a screened Coulomb potential *J. Chem. Phys.* **118** 8207–15
- [34] Heyd J and Scuseria G E 2004 Efficient hybrid density functional calculations in solids: assessment of the Heyd–Scuseria–Ernzerhof screened Coulomb hybrid functional *J. Chem. Phys.* **121** 1187–92
- [35] Heyd J, Scuseria G E and Ernzerhof M 2006 Erratum: ‘hybrid functionals based on a screened Coulomb potential’ (*J. Chem. Phys.* **118**, 8207 (2003)) *J. Chem. Phys.* **124** 219906
- [36] Monkhorst H J and Pack J D 1976 Special points for Brillouin-zone integrations *Phys. Rev. B* **13** 5188–92
- [37] Grimme S, Antony J, Ehrlich S and Krieg H 2010 A consistent and accurate *ab initio* parametrization of density functional dispersion correction (DFT-D) for the 94 elements H–Pu *J. Chem. Phys.* **132** 154104
- [38] Aroyo M I, Kirov A, Capillas C, Perez-Mato J M and Wondratschek H 2006 Bilbao crystallographic server. II. Representations of crystallographic point groups and space groups *Acta Crystallogr. A* **62** 115–28
- [39] Aroyo M I, Perez-Mato J M, Capillas C, Kroumova E, Ivantchev S, Madariaga G, Kirov A and Wondratschek H 2006 Bilbao crystallographic server: I. Databases and crystallographic computing programs *Z. Kristallogr.* **221** 15
- [40] Aroyo M I, Perez-Mato J M, Orobengoa D, Tasci E, De La Flor G and Kirov A 2011 Crystallography online: bilbao crystallographic server *Bulg. Chem. Commun.* **43** 183–97
- [41] Mostofi A A, Yates J R, Pizzi G, Lee Y-S, Souza I, Vanderbilt D and Marzari N 2014 An updated version of wannier90: a tool for obtaining maximally-localised Wannier functions *Comput. Phys. Commun.* **185** 2309–10
- [42] Maintz S, Deringer V L, Tchougréeff A L and Dronskowski R 2013 Analytic projection from plane-wave and PAW wavefunctions and application to chemical-bonding analysis in solids *J. Comput. Chem.* **34** 2557–67
- [43] Maintz S, Deringer V L, Tchougréeff A L and Dronskowski R 2016 LOBSTER: a tool to extract chemical bonding from plane-wave based DFT *J. Comput. Chem.* **37** 1030–5
- [44] Bunge C F, Barrientos J A and Bunge A V 1993 Roothaan–Hartree–Fock ground-state atomic wave functions: slater-type orbital expansions and expectation values for $Z = 2$ –54 *At. Data Nucl. Data Tables* **53** 113–62
- [45] Le Page Y and Saxe P 2002 Symmetry-general least-squares extraction of elastic data for strained materials from *ab initio* calculations of stress *Phys. Rev. B* **65** 104104
- [46] Togo A and Tanaka I 2015 First principles phonon calculations in materials science *Scr. Mater.* **108** 1–5
- [47] Hill R 1952 The elastic behaviour of a crystalline aggregate *Proc. Phys. Soc. A* **65** 349–54
- [48] Yu L and Zunger A 2012 Identification of potential photovoltaic absorbers based on first-principles spectroscopic screening of materials *Phys. Rev. Lett.* **108** 068701
- [49] Engbring J and Fröhlich D 1996 Two-photon absorption and magnetoabsorption of P excitons in β - ZnP_2 *Phys. Status Solidi B* **461** 461–72
- [50] Pauling L and Simonetta M 1952 Bond orbitals and bond energy in elementary phosphorus *J. Chem. Phys.* **20** 29–34
- [51] Pauling L 1960 *The Nature of the Chemical Bond: an Introduction to Modern Structural Chemistry (The George Fisher Baker Non-Resident Lectureship in Chemistry at Cornell University)* (Ithaca, NY: Cornell University Press)
- [52] Dutkiewicz J 1991 The P–Zn (phosphorus–zinc) system *J. Phase Equilib.* **12** 435–8
- [53] Vold C L 1961 The crystal structure of NbZn_2 *Acta Crystallogr.* **14** 1289–90
- [54] Cowley R A 1976 Acoustic phonon instabilities and structural phase transitions *Phys. Rev. B* **13** 4877–85
- [55] Yu C-F, Cheng H-C and Chen W-H 2016 An *ab initio* study of structural, elastic, electronic and thermodynamic properties of triclinic Cu_7In_3 *Mater. Chem. Phys.* **174** 70–80
- [56] Baroni S, De Gironcoli S, Dal Corso A and Giannozzi P 2001 Phonons and related crystal properties from density-functional perturbation theory *Rev. Mod. Phys.* **73** 515–62
- [57] Lukačević I 2011 High pressure lattice dynamics, dielectric and thermodynamic properties of SrO *Physica B* **406** 3410–6
- [58] Stamov I G, Syrbu N N and Zalamai V V 2014 Optical properties and band structure of ZnP_2 - D_4^8 *J. Lumin.* **149** 19–27

- [59] Soshnikov L E, Trukhan V M, Golyakevich T V and Soshnikova H L 2005 Elastic and dielectric properties of $A^II B_2^V$ ($A = \text{Cd}$ or Zn , $B = \text{P}$ or As) single crystals *Crystallogr. Rep.* **50** S37–45
- [60] Samuel V and Rao V J 1989 Optical and valence band studies of ZnP_2 thin films *J. Mater. Res.* **4** 185–8
- [61] Kuzmany H 1998 The dielectric function *Solid-State Spectroscopy* (Berlin: Springer) pp 101–20
- [62] Bercx M, Sarmadian N, Saniz R, Partoens B and Lamoen D 2016 First-principles analysis of the spectroscopic limited maximum efficiency of photovoltaic absorber layers for CuAu-like chalcogenides and silicon *Phys. Chem. Chem. Phys.* **18** 20542–9